Nickel Cysteine Complexes as Anodic Electrocatalysts for Fuel Cells

Dayi Chen,* Fabien Giroud, and Shelley D. Minteer,z**

Departments of Chemistry and Materials Science & Engineering, University of Utah, Salt Lake City, Utah 84112, USA

Compared to platinum, nickel is an inexpensive catalyst that can oxidize methanol in alkaline media. There is a desire to increase nickel loading during electrodeposition for improved performance. In this paper, a nickel cysteine complex (NiCys) is used as the precursor for electrodeposition on glassy carbon electrode surfaces. After optimization of cysteine concentration, the surface concentration of NiOOH on NiCys electrodes characterized by cyclic voltammetry in 0.1 M NaOH can reach 1.28 (± 0.32) $\times 10^{-7}$ mol/cm^2. The large amount of NiOOH on NiCys electrodes provide 5 times the methanol oxidation current compared to Ni electrodes prepared without cysteine as demonstrated by chronoamperometry at 0.7 V vs. Hg/HgO. Atomic force microscopy (AFM), X-ray photoelectron spectroscopy (XPS) and attenuated total reflection Fourier transform infrared (ATR-FTIR) spectroscopy have been applied to examine surface morphologies and structures of NiCys and Ni electrodes. The analysis reveals that cysteine adjusts the solubility of $Ni(OH)_2$ in 0.1 M NaOH, so more uniform and smaller size nanoparticles are electrodeposited on electrode surfaces compared to Ni electrodes.

Manuscript submitted May 9, 2014; revised manuscript received June 6, 2014. Published June 14, 2014.

Fuel cells are a promising energy conversion device to convert chemical energy in a fuel to electrical energy. Nickel-based anodic electrocatalysts are cheaper than conventional precious metal based catalysts and can oxidize various fuels e.g. alcohols, carbohydrates, amino acids and alkanes in alkaline media.[1] Direct methanol fuel cells are attracting more interest, because methanol has a high theoretical energy density and is easy to handle in transportation and storage. In recent years, there has been extensive research on using nickel based catalysts to electro-oxidize methanol. Planar nickel electrodes show poor catalytic activities,[2] so some researchers have focused on dispersing nickel centers in three dimensional structures to increase methanol oxidation current. Based on this concept, many nickel complexes in alkaline solution have been electrodeposited onto glassy carbon electrode surfaces and the electrochemical properties have been examined.[2–14] Nickel macrocyclic complexes, such as nickel porphyrin, cyclam, annulene, salen and cyanine, have been studied. These examples show methanol oxidation currents are five to eighty times higher than their nickel control electrodes.[5,15] However, none of these studies provide a thorough description of the three dimensional structure, i.e. how nickel centers are dispersed by these nickel complexes. It is also not discussed as to how these nickel complexes relate to NiOOH (the catalytically active species) in chemical structure. Very few papers present surface morphology images.[3,4] Most of these nickel complexes have NiOOH surface concentration in the range of 10^{-9} to 10^{-8} mol/cm^2. One of the nickel annulene has reached the highest value of 9.7×10^{-8} mol/cm^2.[16]

We noticed that cysteine can dissolve $Ni(OH)_2$ in 0.1 M NaOH, so cysteine should have a strong interaction with $Ni(OH)_2$. This paper studies the electrodeposition of nickel cysteine in 0.1 M NaOH with different cysteine concentrations. The NiOOH surface concentration in 0.1 M NaOH was measured for each system and catalytic activities for methanol oxidation have also been examined. Atomic force microscopy (AFM), X-ray photoelectron spectroscopy (XPS) and attenuated total reflection Fourier transform infrared (ATR-FTIR) spectroscopy have been performed to characterize surface morphologies and chemical structures of the electrodes to reveal how cysteine affects the electrode properties.

Experimental

Reagents and apparatus.— L-cysteine and nickel (II) chloride (anhydrous, powder, 99.99% trace metals basis) were purchased from Sigma-Aldrich. AS-4, an ionomer that promotes anion (OH^-) exchange, was purchased from Tokuyama Corporation. All solutions were made with ultrapure water (Milli-Q system, 18.2 MΩ•cm) and degassed by nitrogen purging.

The electrochemical experiments were performed with a three-electrode configuration. A Hg/HgO (1M NaOH) electrode was used as the reference electrode and a platinum mesh electrode was used as the counter electrode. The working electrode was a glassy carbon disk electrode (CH Instruments: diameter of 3 mm). Prior to electrode modification, the glassy carbon electrode was soaked in a saturated EDTA solution and stirred overnight to remove nickel residues from previous experiments and then polished with 1 μm and 0.05 μm alumina polish media successively, followed by sonication in ultrapure water and ethanol. Cyclic voltammetry (CV) was performed with a Bio-logic SP-150 potentiostat/galvanostat. Chronoamperometry was carried out with CH Instruments 611C potentiostat. Modified electrode surfaces were characterized by atomic force microscopy (Bruker Dimension Icon-PT atomic force microscope with Peak Force Tapping mode), X-ray photoelectron spectroscopy (Kratos Axis Ultra DLD) and attenuated total reflection Fourier transform infrared spectroscopy (Nicolet iS50). The silicon nitride lever of AFM has a single cantilever with force constant k = 0.4 N/m, resonant frequencies f_0 = 50–90 kHz, radius of curvature of 2 nm. Images were taken with 1 μm size (512 samples/line) at room temperature and analyzed with Nanoscope Analysis software version 1.20. First order flattening was applied to the images. In the XPS experiments, the base chamber pressure was 3×10^{-10} torr. The X-ray source was monochromatized Al K_α radiation ($h\nu$ = 1486.6 eV) at 180 W; the survey and high-resolution spectra (O 1s, C 1s, N 1s, S 2p, Ni 2p) were acquired with pass energies of 160 and 40 eV, respectively. Spectra were analyzed with CasaXPS software. 284.8 eV of physisorbed C1s was used to correct the binding energy. Shirley-type background was subtracted in the spectra. Each ATR-FTIR spectrum took 64 scans and the resolution was 4 cm^{-1}, resulting in a data spacing of 1.928 cm^{-1}.

Electrodes preparation.— Nickel loading dependency on cysteine concentration was studied in this work. In the precursor, Ni^{2+} ($NiCl_2$) concentration was held at 0.01 M and cysteine concentrations were varied from 0.005 M to 0.06 M. Only 0.01 M $NiCl_2$ was also studied as a control. The nickel cysteine solutions were stirred for 3.5 hours prior

*Electrochemical Society Student Member.
**Electrochemical Society Fellow.
zE-mail: minteer@chem.utah.edu

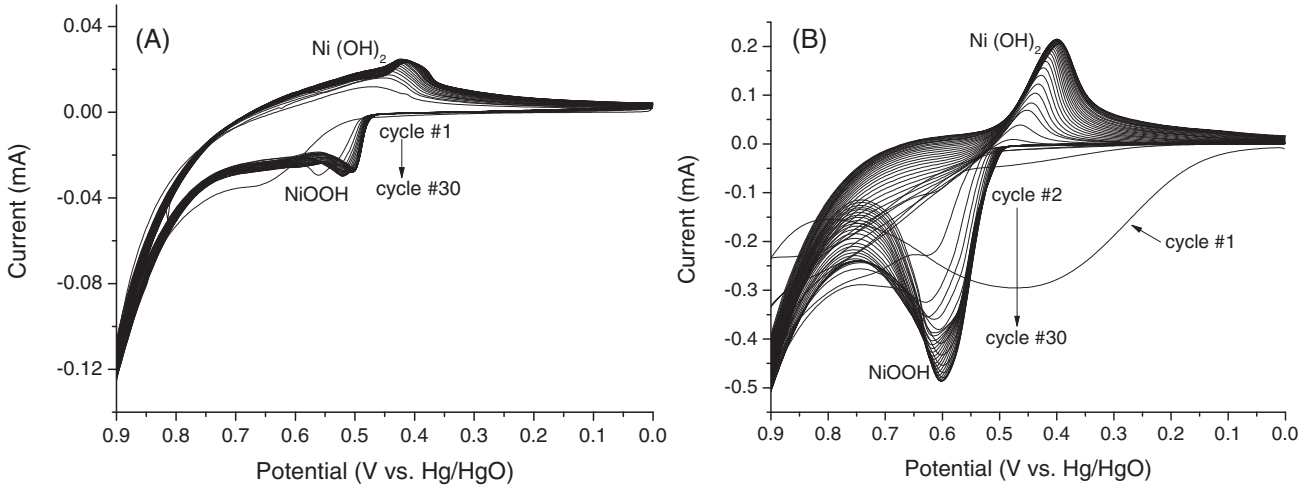

Figure 1. Nickel catalyst deposition: representative cyclic voltammograms of Ni and NiCys AS-4 electrodes in 0.1 M NaOH. Scan rate 50 mV/s, 30 cycles. (A) 0.01 M $NiCl_2$ precursor. (B) 0.01 M $NiCl_2$ and 0.05 M cysteine precursor.

to using to ensure complex formation. 5 μL nickel cysteine complex (with different nickel cysteine ratios) solution or $NiCl_2$ solution was drop-casted onto glassy carbon electrode surfaces. After the solution was dry, 3.54 μL of AS-4 (an ionomer that promotes OH^- exchange) solution was drop-casted on top of it and allowed to dry overnight. Nickel based catalysts were evaluated by cyclic voltammetry (CV) in 0.1 M NaOH for 30 cycles from 0 V to 0.9 V vs. Hg/HgO at a scan rate of 50 mV/s. Electrodes were then tested in 0.1 M NaOH with 0.1 M methanol with CVs for 30 cycles as well. For surface characterizations, glassy carbon plates instead of glassy carbon electrodes were used and AS-4 solution was not applied during preparation.

Chronoamperometry.— Chronoamperometry with methanol concentrations from 0 to 1 M was performed in 0.1 M NaOH at 0.7 V vs. Hg/HgO while stirring at a constant controlled rate. In each experiment, the charging current was allowed to dissipate for >1000 s, and for each methanol concentration, there was at least 300 seconds between injections to make sure steady-state current is reached.

Results and Discussion

Cysteine effects on nickel catalyst deposition.— Nickel based catalysts were deposited onto AS-4 coated glassy carbon electrode surfaces by cyclic voltammetry in 0.1 M NaOH for 30 cycles. According to literature,[17,18] C-O-Ni oxo bridges are formed during this process, so that the catalysts are attached to the electrode surfaces and the pair of redox peaks in the CVs are the $Ni(OH)_2$ and NiOOH peaks. The redox reaction of Ni could be expressed as:

$$Ni(OH)_2 + OH^- \rightarrow NiOOH + H_2O + e^- \quad [1]$$

The current increase after 0.7 V in the CVs is from oxygen evolution:[16]

$$4NiOOH \rightarrow 4NiO + 4^{\bullet}OH \rightarrow 4NiO + O_2 + 2H_2O \quad [2]$$

Without cysteine (Figure 1A), the NiOOH peak current does not increase from cycle 2 to cycle 30. With cysteine present (Figure 1B), the first cycle shows a peak around 0.45 V resulting from cysteine oxidation.[19] After irreversible cysteine oxidation in the first one or two cycles (depending on the amount of cysteine), nickel peaks are observed which increase as the cycle number increase. We scanned 30 cycles in order to have stable peak currents.

The 30th cycle of Ni and NiCys deposition in 0.1 M NaOH are shown in Figure 2A. When cysteine concentration increases, NiOOH peak current also increases, indicating more Ni centers on the electrode surfaces are accessible by OH^-.

NiOOH surface concentration (Γ) is calculated by equation 3:[4]

$$\Gamma = \frac{Q}{n\mathrm{FA}} \quad [3]$$

where F is Faraday's constant, A is the geometric surface area of the glassy carbon electrodes and n is the number of electrons transferred during $Ni(OH)_2$ to NiOOH, which is assumed to be 1 here. Q is the charge under the NiOOH peak, and the baseline is chosen as shown in Figure S1. By this method, the charge resulting from side reactions, e.g. oxygen evolution, can be subtracted (see supporting information[20] Figure S1). The number of electrons produced by cysteine oxidation is also converted by equation 3, assuming n = 1, so that the relationship between NiOOH amount and cysteine oxidation can be revealed. The results are plotted in Figure 2B. Both the amount of NiOOH and the amount of oxidized cysteine increase as initial cysteine concentration increases, but they follow different trends. In Figure 2B, the surface concentrations of cysteine oxidation are below NiOOH when cysteine concentration is lower than 0.02 M, while when cysteine concentration is above 0.04 M, the case is the opposite. There could be some transition between 0.02 M and 0.04 M cysteine. The significance of this work is the NiOOH amount reaches 12.8 (± 3.2) × 10^{-8} mol/cm^2 when cysteine concentration is 0.06 M. To our knowledge, the previously reported highest NiOOH amount on glassy carbon electrode prepared by nickel complexes is 9.7 × 10^{-8} mol/cm^2,[16] so our NiCys AS-4 electrodes have achieved comparable nickel loading to the highest reported one.

Possible structures of electrodeposited Ni and NiCys catalysts.— Ni (0.01 M $NiCl_2$), and Ni1Cys5 (0.01 M $NiCl_2$ /0.05 M cysteine) modified glassy carbon plates were prepared without the AS-4 polymer layer on glassy carbon surfaces and characterized by X-ray photoelectron spectroscopy (XPS). As shown in Figure 3, carbon, oxygen and nickel are detected in the Ni (0.01 M $NiCl_2$) sample, while carbon, oxygen, nitrogen, sulfur and nickel are detected in Ni1Cys5 (0.01 M $NiCl_2$ /0.05 M cysteine) sample. The Ni to S ratio is about 1:1 based on the quantitative analysis, suggesting the sample contains equivalent nickel ions and cysteine oxidation product, although in the precursor, the Ni to cysteine ratio is 1:5.

There is no apparent binding energy difference in the two Ni 2p spectra, indicating the oxidation states of Ni in the Ni and Ni1Cys5 samples are the same and fall in the binding energy range of NiO, $Ni(OH)_2$ and NiOOH.[21] The peak around 289 eV in the carbon 1s spectrum of the Ni sample suggests some carbon on the glassy carbon plate is oxidized to carboxylate and/or CO_3^{2-} has contaminated the sample in the alkaline solution during sample preparation.[22]

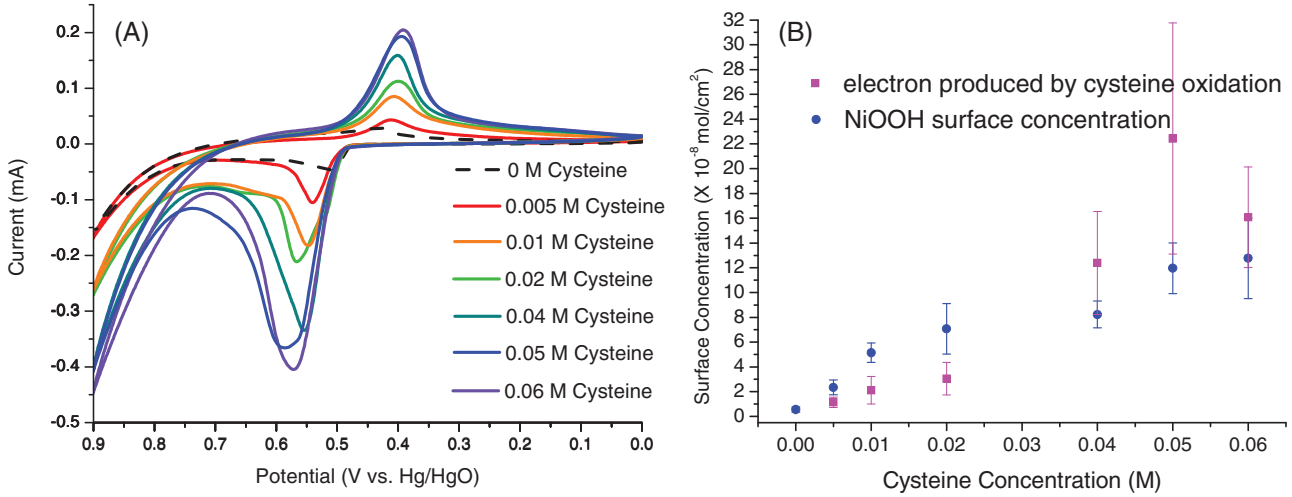

Figure 2. Nickel catalysts deposition: (A) Representative 30th cycle of cyclic voltammograms from scanning Ni and NiCys AS-4 electrodes in 0.1 M NaOH. Scan rate 50 mV/s. Cysteine concentration increased from 0 M to 0.06 M and $NiCl_2$ concentration was kept at 0.01 M. (B) Electrons produced by cysteine oxidation and NiOOH surface concentration versus cysteine concentration. In this plot the number of electrons produced by cysteine oxidation is converted by equation 3, assuming n = 1, so it has the same unit as the NiOOH surface concentration.

Based on the following ATR-FTIR data, both assignments are possible. The deconvolution spectra (see supporting information[20] Figure S2) of O 1s show both the Ni and Ni1Cys5 sample contain hydroxide and the Ni sample also contains small amounts of oxide. The binding energy of the N 1s spectrum and one of the O 1s deconvolutional component in Ni1Cys5 sample fit the profile of $–NH_2$ and $–COO^-$ groups, respectively.[20,22] The binding energy of sulfur is in the range of S = O group, suggesting sulfur is oxidized.[23] To summarize, the Ni sample contains nickel hydroxide and a small amount of nickel oxide, whereas the Ni1Cys5 sample contains nickel hydroxide and the oxidized cysteine product in a ratio of Ni:Cys of 1:1.

More structural information can be revealed via ATR-FTIR spectroscopy (see supporting information[20] Figure S3). The Ni and Ni1Cys5 samples were prepared on glassy carbon plates without the AS-4 layer. Figure S3 shows the FTIR spectra of bare glassy carbon plate, electrodeposited Ni sample and chemically prepared Ni1Cys5 sample (the electrodeposited Ni1Cys5 sample was too thin to be probed by ATR-FTIR). In the spectra of the Ni and Ni1Cys5 samples, the peak around 466 cm^{-1} is the Ni-O stretching mode. The broad and intense peak around 3200 cm^{-1} can be assigned to O-H stretching mode. These suggest both Ni and Ni1Cys5 samples could have formed layered nickel hydroxide structure.[24]

In the Ni spectrum, the strong peak around 1359 cm^{-1} could be the stretching mode of CO_3^{2-} groups intercalated between $Ni(OH)_2$ layers. A small amount of $–COO^-$ stretching modes around 1610–1400 cm^{-1} could be buried in the broad 1359 cm^{-1} peak. The main peaks of this spectrum are almost identical to the spectrum of electrodeposited CO_3^{2-} intercalated α-$Ni(OH)_2$ reported by M. Figlarz et al.[24] When comparing the cysteine sample and Ni1Cys5 sample in Figure S3B, it shows the –SH stretching at 2540 cm^{-1} in the cysteine sample disappeared in the NiCys5 sample. Instead, NiCys5 shows the –S–O stretching mode at 1079 cm^{-1}.[25,26] This suggests –SH has been oxidized to –SO during sample preparation. Since XPS results show the electrodeposited Ni1Cys5 sample also shows sulfur has been oxidized to sulphonate, it can be concluded that cysteine is very easy to oxidize in the presence of Ni ions in an alkaline environment. The oxidized structure is shown in Figure 4. The 1506 cm^{-1} peak and 1476 cm^{-1} peak are $\delta_s(NH_3^+)$ and $\nu_{as}(COO^-)$, respectively. In the Ni1Cys5 sample, the alkaline environment causes $–NH_3^+$ to be deprotonated, so the peak disappeared. The peak shift from 1476 cm^{-1} to 1458 cm^{-1} indicates Ni^{2+} coordinating to $–COO^-$. Based on the structure in Figure 4 and the information from FTIR, Ni ions probably coordinate to the $–COO^-$ and $–SO_3^-$ groups.

Bode's representation of nickel oxyhydroxides and nickel hydroxides[27] has well represented the different phases of $Ni(OH)_2$ and NiOOH. All of these nickel hydroxides and oxyhydroxides have layered structures and the distance (d) between two adjacent layers in α-$Ni(OH)_2$, γ-NiOOH, β-$Ni(OH)_2$ and β-NiOOH are 8.0 Å, 6.9 Å, 4.6 Å and 4.84 Å, respectively. Normally, the charge and discharge conversion happens between α-$Ni(OH)_2$ and γ-NiOOH or between β-$Ni(OH)_2$ and β-NiOOH. If the charge and discharge conversion is between α-$Ni(OH)_2$ and β-NiOOH or between β-$Ni(OH)_2$ and γ-NiOOH, there will be swelling or volume expansion of the nickel film, making the catalyst unstable. Figlarz et al. has studied the species intercalated between chemically precipitated nickel hydroxide layers.[28] They found out their sample is α-$Ni(OH)_2$ and that anions, e.g. NO_3^- and CO_3^{2-}, as well as water molecules can intercalate between the layers. The formula can be written as $Ni(OH)_{2-x}(A)_y(B)_z \bullet nH_2O$, where A and B can be mono and divalent anions, respectively, and y + 2z = x.[24] Larger anions, e.g. acetate, succinate, glutarate, adipate, can intercalate between hydroxide layers and there is a linear relationship between the intersheet distance (d) and the number of carbon atoms of the carboxylate ions (i.e. the length of the ions).[28] They also studied the difference between electrodeposited and chemically precipitated CO_3^{2-} intercalated $Ni(OH)_2$. It turns out both of them are α-$Ni(OH)_2$ and the intersheet distance of electrodeposited α-$Ni(OH)_2$ (7.6 Å) is slightly smaller than chemical precipitated α-$Ni(OH)_2$ (8.1 Å), probably due to the slightly lower hydration degree.[24] Since electrodeposition and chemical precipitation can lead to similar product structure and the intersheet distance has a dependence on intercalated ion size, our newly prepared Ni catalyst could also be a CO_3^{2-} intercalated α-$Ni(OH)_2$ with intersheet distance around 7.6 Å and the Ni1Cys5 catalyst could be a oxidized cysteine intercalated α-$Ni(OH)_2$ with intersheet distance around 11.5 Å (the length of oxidized cysteine is about 6 Å, almost identical to the length of succinate and the intersheet distance of succinate intercalated α-$Ni(OH)_2$ is about 11.5 Å. The lengths are measured with ChemBio3D Ultra 12.0. Default MM2 job had been run to minimize the energy of the structures and the lengths are measured between two negatively charged groups at the ends of the structures). Based on the XPS and FTIR data as well as the deduction above, the possible structures of our newly prepared Ni and NiCys samples are shown in Figure 5.

The phase of the prepared catalyst is important for its performance. Normally the charge and discharge conversion happens between α-$Ni(OH)_2$ and γ-NiOOH or between β-$Ni(OH)_2$ and β-NiOOH. γ-NiOOH has many advantages over β-NiOOH for methanol oxidation.

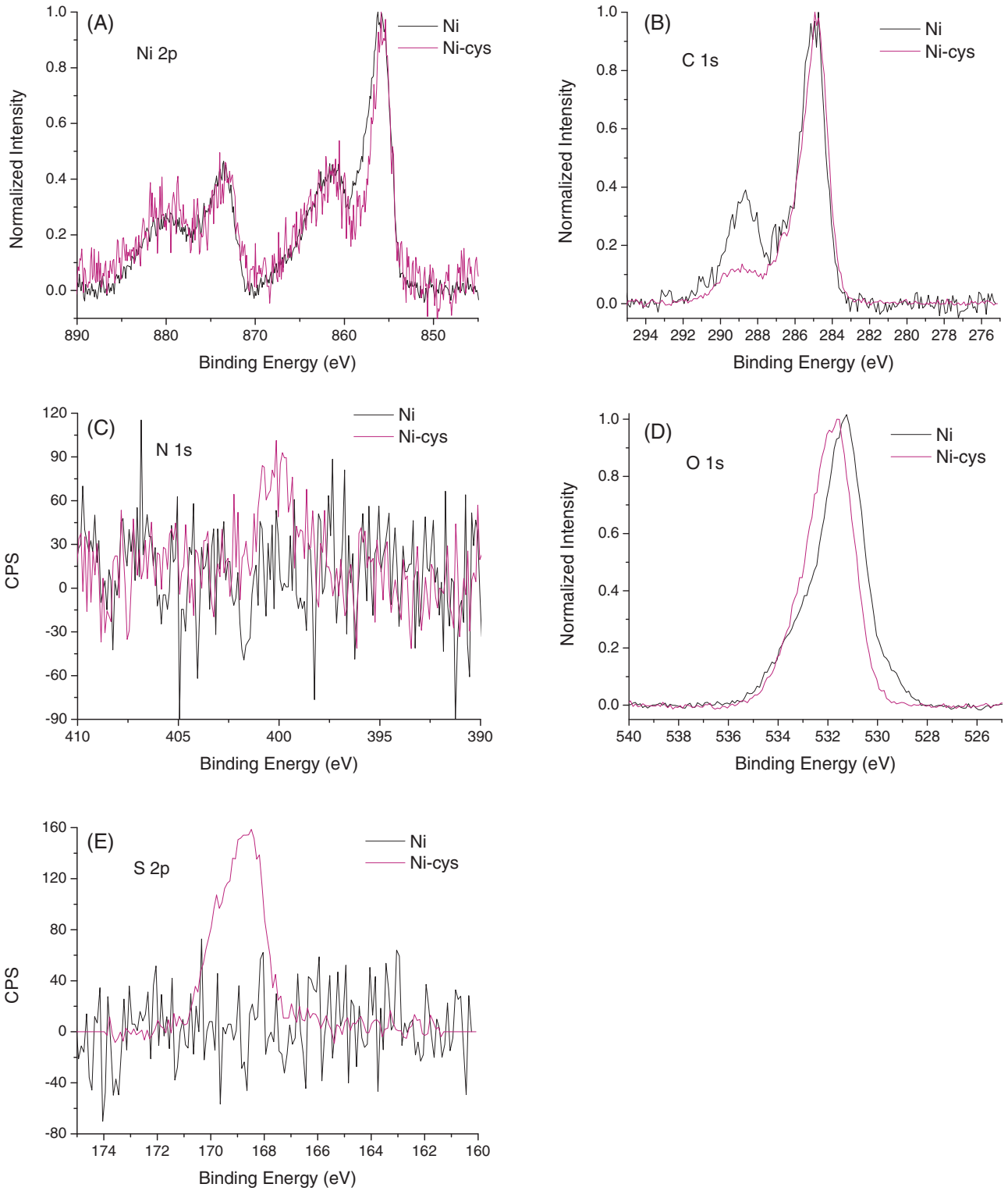

Figure 3. XPS spectra (subtracted the Shirley backgrounds, and for easy comparison the peaks' shapes, nickel 2p, carbon 1s and oxygen 1s peaks were normalized with their own highest peak intensities): (A) Nickel 2p. (B) Carbon 1s. (C) Oxygen 1s. (D) Nitrogen 1s. (E) Sulfur 2p.

The intersheet distance of γ-NiOOH is about 2 Å larger than β-NiOOH and the oxidation state of Ni in γ-NiOOH is 3.67, 0.67 higher than in β-NiOOH.[29] The looser packing of γ-NiOOH than β-NiOOH in agglomerates can provide more porosity and the higher oxidation state gives higher discharge electrochemical capacity.[30] Oxygen evolution consumes NiOOH that could have been used to catalyze methanol oxidation and the oxygen bubble formed by oxygen evolution might cause the catalysts to fall from the electrode surfaces. β-NiOOH has been shown to be more active than γ-NiOOH for oxygen evolution.[29] Moreover, Barnard et al.'s study has shown the formal potential of the α-$Ni(OH)_2$ / γ-NiOOH couple (0.392–0.440 V vs. Hg/HgO/KOH) is lower than the β-$Ni(OH)_2$ / β-NiOOH couple (0.443–0.470 V vs. Hg/HgO/KOH). This also means methanol can be oxidized at lower potential with the α-$Ni(OH)_2$ / γ-NiOOH couple than with the

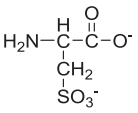

Figure 4. The possible structure of oxidized cysteine in the Ni1Cys5 sample.

β-$Ni(OH)_2$ / β-NiOOH couple,[31] so preparing stable α-$Ni(OH)_2$ instead of β-$Ni(OH)_2$ will improve catalyst performance and benefit methanol fuel cell applications.

Surface morphology of the catalysts.— Surface morphology of the catalysts was probed by AFM to reveal other differences between Ni and NiCys samples (see supporting information[20] Figure S4). Ni (0.01 M $NiCl_2$), Ni1Cys0.5 (0.01 M $NiCl_2$ /0.005 M cysteine), Ni1Cys2 (0.01 M $NiCl_2$ /0.02 M cysteine) and Ni1Cys5 (0.01 M $NiCl_2$ /0.05 M cysteine) were prepared on glassy carbon (GC) plates without the AS-4 polymer layer coating on the top. The root mean square roughness (R_q) of the samples are 0.577 nm (bare glassy carbon plate), 10.7 ± 2.4 nm (Ni1Cys0.5), 10.0 ± 1.6 nm (Ni1Cys2), 6.8 ± 1.4 nm (Ni1Cys5), 33.5 ± 3.9 nm (Ni with large aggregates, e.g. Figure S4 E) and 4.5 ± 0.1 nm (Ni with thin layer, e.g. Figure S4 F).

Section analysis shows both the Ni and NiCys modified surfaces have nanoparticles on the surface. The Ni1Cys5 surfaces have these particles distributed quite uniformly with diameters of 20–35 nm and heights of 5–20 nm. The Ni surfaces also have these particles, but the surfaces are heterogeneous - the particles either form large aggregates (Figure S4 E) with heights over 100 nm or the particles cannot fully cover the surfaces (Figure S4 F). The particle size of the Ni1Cys0.5 and Ni1Cys2 surfaces is between the Ni and Ni1Cys5 surfaces. The majority of the particles are 25–40 nm in diameter and 10–20 nm in height. Besides, about 25% of the particles found on Ni1Cys0.5 surfaces are 50–60 nm in diameter and 20–30 nm in height.

The trend is as the cysteine concentration increases, the heterogeneity of the surface and the particle size decrease. This could be due to the solubility of $Ni(OH)_2$ in 0.1 M NaOH with different cysteine concentrations (see supporting information[20] Figure S5). When there is no cysteine present, OH^- precipitates Ni^{2+} from $NiCl_2$ immediately. Correspondingly, when Ni AS-4 electrodes are prepared by electrodeposition, the NiOOH is all deposited during the first CV, and further scans do not increase the NiOOH peak current as shown in Figure 1A. On the other hand, cysteine can dissolve $Ni(OH)_2$ in alkaline media. The presence of cysteine can probably decrease the nickel precipitation rate to make the deposition more uniform, so the NiOOH peak current of NiCys AS-4 electrodes increases during the first several cycles in contrast to Ni AS-4 electrodes (Figure 1B). Furthermore, as pointed in Figure 2B, there could be some transition between 0.02 M and 0.04 M cysteine, e.g. when cysteine concentration is or below 0.02 M, cysteine oxidation products only intercalate between $Ni(OH)_2$ layers but when cysteine concentration is or above 0.04 M, there is some cysteine oxidation products adsorbed onto $Ni(OH)_2$ surfaces besides those intercalate between $Ni(OH)_2$ layers, so in the case of Ni1Cys5, the large amount of cysteine might partially dissolve the deposited particles causing the particle size of Ni1Cys5 to be the smallest.

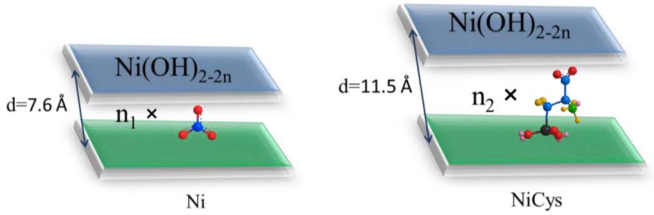

Figure 5. Possible structures of Ni and NiCys samples, newly prepared by electrodeposition.

These samples are not covered by the AS-4 layer. According to the results from cyclic voltammetry, Ni1Cys5 samples have about 25% nickel loading (NiOOH surface concentration) compared to Ni samples, both without the AS-4 layer, and 10 times higher nickel loading compared to Ni samples when they are both covered with the AS-4 layer (see supporting information[20] Figure S6). It is probable that when Ni1Cys5 sample is prepared without the AS-4 layer, only the very thin layer closest to glassy carbon surfaces is left. When they are prepared with the AS-4 layer, nickel complexes are less able to leach so the amount of Ni will be about the same among all Ni and NiCys samples. In this situation, smaller particle size will have higher surface area. This explains why Ni1Cys5 AS-4 electrodes have the highest NiOOH surface concentration among these 4 samples. The effect of AS-4 layer on catalyst performance is further discussed in the supporting information[20] Figure S7. AFM analysis suggests adding more cysteine in the Ni-cysteine precursor will result in smaller nanoparticles and more homogeneous distribution on the surface. The particle size and surface homogeneity could affect the catalytic efficiency.

Methanol oxidation by Ni and NiCys electrodes.— As shown in Figure 6A, the large peak around 0.7 V is the methanol oxidation peak. The reaction is:[16]

$$\text{NiOOH} + \text{fuel} \rightarrow \text{Ni(OH)}_2 + \text{oxidation product} \quad [4]$$

Since higher cysteine concentration provides higher NiOOH surface concentration, electrodes with higher cysteine concentration also produce higher methanol oxidation current. This is further investigated by chronoamperometry. Figure 6B is a representative example of the amperometric experiments. The arrows represent each methanol injection. After adding methanol, the current increased immediately. At high methanol concentrations, the nickel centers were saturated and the current did not increase further. Figure 6C shows the current density (Calculated from the geometric surface area of the glassy carbon electrodes) change with increasing methanol concentration and the maximum methanol oxidation current is reached at 0.3 M methanol. The methanol oxidation current increases as cysteine concentration in the precursor raises due to the increasing NiOOH surface concentration. The current has about 5 times enhancement at 0.3 M methanol when comparing Ni1Cys6 AS-4 to Ni AS-4 electrodes. This shows that the presence of cysteine can improve the methanol oxidation current. The methanol oxidation current decrease when methanol concentration is higher than 0.3 M with Ni1Cys4, Ni1Cys5 and Ni1Cys6 AS-4 electrodes. This current decrease is probably due to "poisoning" from some methanol oxidation intermediates. Detailed discussion of this phenomenon is in supporting information (Figure S7).[20]

Platinum has been considered as the most promising anodic catalyst candidate among pure metals for application in direct methanol fuel cells.[32] Methanol oxidation starts at the onset of OH^- adsorption on platinum. Tripkovic et al.'s study shows in 0.1 M NaOH OH^- adsorption starts at around 0.45 V (vs. RHE) on platinum deposited glassy carbon electrodes. Their platinum electrodes have 8 mA/cm^2 current density maximum at about 0.95 V (vs. RHE) with cyclic voltammetry (scan rate 50 mV/s) when oxidizing 0.5 M methanol in 0.1 M NaOH.[33] On the other hand, methanol oxidation with NiOOH initiates after NiOOH is produced. The potential of the onset of NiOOH production is around 0.6 V (vs. RHE), so methanol is oxidized at higher potential on NiOOH than on platinum. The cyclic voltammograms of 0.1 M methanol oxidized in 0.1 M NaOH with Ni1Cys6 AS-4 electrodes show 10.2(± 1.7) mA/cm^2 current density maximum at about 0.92(±0.3) V (vs. RHE) with scan rate 50 mV/s. Moreover, if the current production is converted to current per catalyst mass (A/g, using the NiOOH surface concentration to calculate the mass of NiOOH), Ni1Cys6 AS-4 electrodes produce current about 1240 (± 320) A/g with 0.3 M methanol in 0.1 M NaOH at 0.82 V (vs. RHE) calculated from chronoamperometry data. Some studies of platinum or platinum ruthenium alloy only have a current range from 300 A/g to 900 A/g with 1 M methanol in acidic environments,[34] so nickel cysteine complexes are competitive anodic electrocatalysts for methanol fuel cells.

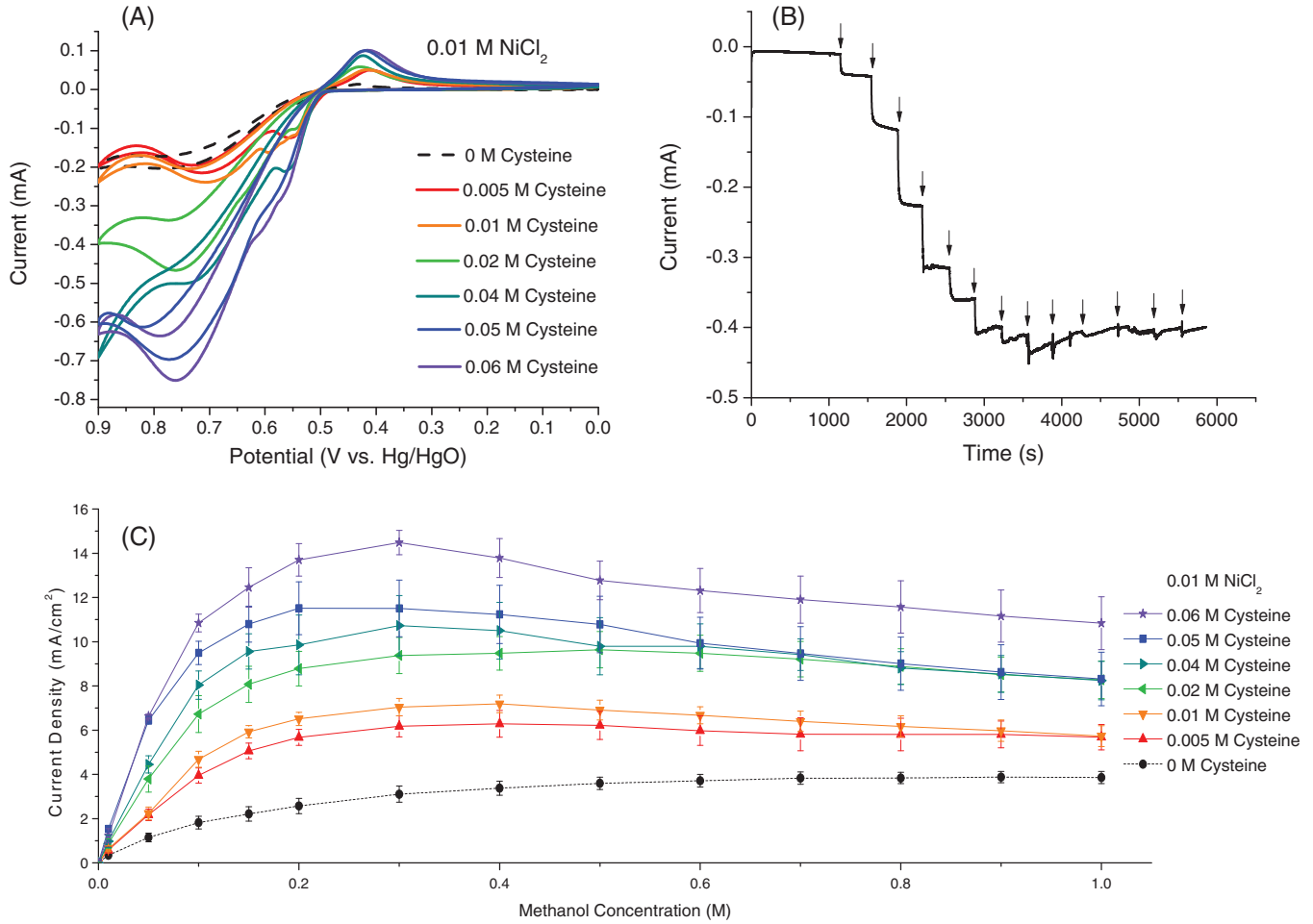

Figure 6. (A) Representative cyclic voltammograms of Ni and NiCys AS-4 electrodes in 0.1 M NaOH and 0.1 M methanol, scan rate 50 mV/s. (B) Chronoamperometric response for a Ni1Cys0.5 (0.01 M $NiCl_2$ and 0.005 M Cysteine) AS-4 electrode in 0.1 M NaOH and increasing concentrations of methanol at 0.7 V (vs. Hg/HgO). The methanol concentration ranges from 0 M to 1 M. (C) Calibration curves of methanol oxidation for Ni and NiCys AS-4 electrodes. Data were calculated from chronoamperometry experiments (e.g. Figure 6B).

Conclusions

NiCys AS-4 electrodes have achieved comparable NiOOH surface concentration to the highest reported nickel complexes on glassy carbon electrodes. Compared to Ni AS-4 electrodes, NiCys AS-4 electrodes can enhance methanol oxidation current by 5 times in 0.3 M methanol, because of the high NiOOH surface concentration. The high methanol oxidation current production makes nickel cysteine complexes competitive anodic electrocatalysts for methanol fuel cells. Surface characterization shows that cysteine adjusts the solubility of $Ni(OH)_2$ in 0.1 M NaOH, so more uniform and smaller size nanoparticles are electrodeposited on electrode surfaces. The surface area of the catalysts is enlarged thus more $Ni(OH)_2$ are accessible to OH^- to form NiOOH. This benefits the methanol oxidation process.

Acknowledgment

The authors thank the National Science Foundation (Grants #1057597) for funding and Dr. Paulo Perez in Nanofab lab of University of Utah for doing X-ray photoelectron spectroscopy (XPS) experiments.

References

1. D. Chen, G. G. W. Lee, and S. D. Minteer, *ECS Electrochemistry Letters*, **2**, F9 (2012).
2. A. N. Golikand, M. Asgari, and M. G. Maragheh, et al, *Journal of Electroanalytical Chemistry*, **588**, 155 (2006).
3. T. R. I. Cataldi, E. Desimoni, and G. Ricciardi, et al, *Electroanalysis*, **7**, 435 (1995).
4. S. M. Golabi and A. Nozad, *Electroanalysis*, **16**, 199 (2004).
5. M. Revenga-Parra, T. García, and E. Lorenzo, et al, *Sensors and Actuators B: Chemical*, **130**, 730 (2008).
6. S. P. Trevin, F. Bedioui, and M. G. G. Villegas, et al, *Journal of Materials Chemistry*, **7**, 923 (1997).
7. A. Ciszewski and G. Milczarek, *Journal of Electroanalytical Chemistry*, **413**, 137 (1996).
8. T. R. I. Cataldi, D. Centoze, and G. Ricciardi, *Electroanalysis*, **7**, 312 (1995).
9. A. Ciszewski and G. Milczarek, *Journal of Electroanalytical Chemistry*, **426**, 125 (1997).
10. M. Jafarian, M. A. Haghighatbin, and F. Gobal, et al, *Journal of Electroanalytical Chemistry*, **663**, 14 (2011).
11. M. S. Ureta-Zañartu, A. Alarcón, and G. Muñoz, et al, *Electrochimica Acta*, **52**, 7857 (2007).
12. R. Ojani, J.-B. Raoof, and S. R. H. Zavvarmahalleh, *Electrochimica Acta*, **53**, 2402 (2008).
13. A. Ciszewski and I. Stepniak, *Electrochimica Acta*, **76**, 462 (2012).
14. L. Zheng and J.-F. Song, *Journal of Solid State Electrochemistry*, **14**, 43 (2010).
15. J. Taraszewska and G. Roslonek, *Journal of Electroanalytical Chemistry*, **364**, 209 (1994).
16. I. G. Casella, T. R. I. Cataldi, and A. M. Salvi, et al, *Analytical Chemistry*, **65**, 3143 (1993).
17. G. Roslonek and J. Taraszewska, *Journal of Electroanalytical Chemistry*, **325**, 285 (1992).
18. G. Zhou, D.-W. Wang, and L.-C. Yin, et al, *ACS Nano*, **6**, 3214 (2012).
19. D. Jia, F. Li, and L. Sheng, et al, *Electrochemistry Communications*, **13**, 1119 (2011).
20. D. Chen, F. Giroud, and S. D. Minteer, Supporting Information, in (2014).
21. M. C. Biesinger, B. P. Payne, and L. W. M. Lau, et al, *Surface and Interface Analysis*, **41**, 324 (2009).
22. A. V. Naumkin, A. Kraut-Vass, and S. W. Gaarenstroom, et al, NIST Standard Reference Database 20, Version 4.1, in, the National Institute of Standards and Technology, http://srdata.nist.gov/xps/ (2012).

23. K. Wang, L. Hong, and Z.-L. Liu, *Industrial and Engineering Chemistry Research*, **47**, 6517 (2008).
24. F. Portemer, A. Delahaye-Vidal, and M. Figlarz, *Journal of The Electrochemical Society*, **139**, 671 (1992).
25. Z.-Y. Wang, G. Li, and Z.-G. Sun, *Wuli Huaxue Xuebao*, **29**, 2422 (2013).
26. S. Biswas, J. Zhang, and Z. Li, et al, *Dalton Trans*, **42**, 4730 (2013).
27. H. Bode, K. Dehmelt, and J. Witte, *Electrochimica Acta*, **11**, 1079 (1966).
28. P. Genin, A. Delahaye-Vidal, and F. Portemer, et al, *European Journal of Solid State and Inorganic Chemistry*, **28**, 505 (1991).
29. B. S. Yeo and A. T. Bell, *The Journal of Physical Chemistry C*, **116**, 8394 (2012).
30. B. B. Ezhov and O. G. Malandin, *Journal of The Electrochemical Society*, **138**, 885 (1991).
31. R. Barnard, C. F. Randell, and F. L. TYE, *Journal of Applied Electrochemistry*, **10**, 109 (1980).
32. A. Chen and P. Holt-Hindle, *Chemical Reviews*, **110**, 3767 (2010).
33. A. V. Tripković, K. D. Popović, and J. D. Lović, et al, *Journal of Electroanalytical Chemistry*, **572**, 119 (2004).
34. L. A. Hutton, M. Vidotti, and A. N. Patel, et al, *The Journal of Physical Chemistry C*, **115**, 1649 (2011).